DOI: 10.1002/chem.200601843

Polymorphism of *N*,*N*′′-Diacetylbiuret Studied by Solid-State ^{13}C and ^{15}N NMR Spectroscopy, DFT Calculations, and X-ray Diffraction

Sven Macholl,*[a, b] Dieter Lentz,[a] Frank Börner,[c] and Gerd Buntkowsky*[d]

Abstract: The molecular configuration and crystal structure of solid polycrystalline *N*,*N*′′-diacetylbiuret (DAB), a potential nitrogen-rich fertilizer, have been analyzed by a combination of solid- and liquid-state NMR spectroscopy, X-ray diffraction, and DFT calculations. Initially a pure NMR study ("NMR crystallography") was performed as available single crystals of DAB were not suitable for X-ray diffraction. Solid-state ^{13}C NMR spectra revealed the unexpected existence of two polymorphic modifications (α- and β-DAB) obtained from different chemical procedures. Several NMR techniques were applied for a thorough characterization of the molecular system, revealing chemical shift anisotropy (CSA) tensors of selected nuclei in the solid state, chemical shifts in the liquid state, and molecular dynamics in the solid state. Dynamic NMR spectroscopy of DAB in solution revealed exchange between two different configurations, which raised the question, is there a correlation between the two different configurations found in solution and the two polymorphic modifications found in the solid state? By using this knowledge, a new crystallization protocol was devised which led to the growth of single crystals suitable for X-ray diffraction. The X-ray data showed that the same symmetric configuration is present in both polymorphic modifications, but the packing patterns in the crystals are different. In both cases hydrogen bonds lead to the formation of planes of DAB molecules. Additional symmetry elements, a twofold screw in the case of α-DAB and a *c*-glide plane in the case of β-DAB, lead to a more symmetric (α-DAB) or asymmetric (β-DAB) intermolecular hydrogen-bonding pattern for each molecule.

Keywords: ab initio calculations · hydrogen bonds · polymorphism · solid-state NMR spectroscopy · X-ray diffraction

Introduction

N,*N*′′-Diacetylbiuret (=1,5-diacetylbiuret, DAB, $[CH_3(C{=}O)NH(C{=}O)]_2NH$, see Figure 1) is a potential long-term, nitrogen-rich fertilizer. As such it exhibits a rather low solubility in water. As solubility often goes hand-in-hand with poor crystallizing behavior, efficient screening of such compounds necessitates the understanding of solubility and the elucidation of molecular configuration/conformation and intermolecular arrangement (hydrogen bonds,[1] supramolecular structure[2–4]). This information can be applied in a bottom-up approach to fine control of structural properties, that is, to crystal engineering.[5] This analysis is of special interest as often polymorphs, pseudopolymorphs, and/or solvates (hydrates) coexist, exhibiting different physicochemical properties including solubility. These different forms of solids are treated as independent substances, for example, in patent law. Prominent examples with huge economic consequences can be found among pharmaceutical products and pigments (see refs. [6–10] and references therein). Several aspects of polymorphism, like thermodynamic properties and molecular structure, can be found in the literature, for example, in refs. [11,12]. A routine technique for gathering detailed information on structures is X-ray diffraction of single crystals. But there exist a large number of organic compounds like

[a] Dr. S. Macholl, Prof. Dr. D. Lentz
Institut für Chemie und Biochemie, Freie Universität
Berlin Fabeckstrasse 34–36/Takustrasse 3, 14195 Berlin (Germany)
Fax:(+49) 30-8385-3310
E-mail: lentz@chemie.fu-berlin.de

[b] Dr. S. Macholl
Present address: GE Healthcare, The Grove Centre
White Lion Road, Amersham, Bucks, HP7 9LL (UK)
E-mail: sven.macholl@ge.com

[c] Dr. F. Börner
Present address: Fraunhofer-Institut für Angewandte Polymerforschung
Postfach 126, 14476 Golm (Germany)

[d] Prof. Dr. G. Buntkowsky
Institut für Physikalische Chemie der
Friedrich-Schiller-Universität Jena
Helmholtzweg 4, 07743 Jena (Germany)
Fax (+49) 3641-948-302
E-mail: gerd.buntkowsky@uni-jena.de

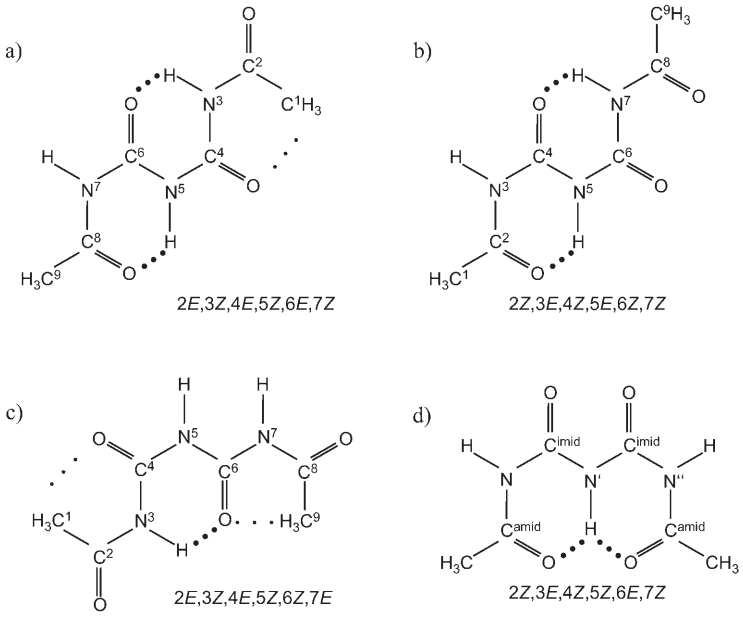

Figure 1. Molecular structures of *N*,*N*″-diacetylbiuret (DAB) from ab initio calculations, shown as selected resonance structures and in the order of increasing electron energy. a) Configuration (2*E*,3*Z*,4*E*,5*Z*,6*E*,7*Z*) (the most stable structure). b) Configuration (2*Z*,3*E*,4*Z*,5*E*,6*Z*,7*Z*). c) Configuration (2*E*,3*Z*,4*E*,5*Z*,6*Z*,7*E*). d) Configuration (2*Z*,3*E*,4*Z*,5*Z*,6*E*,7*Z*). In structures a, b, and c, the numbering of the backbone carbon and nitrogen atoms is given, in structure d the N, N′, N″, C_{amide}, and C_{imide} atoms are labeled as such. N–H···O hydrogen bonds are indicated with bold points and C–H···O hydrogen bonds with fine points.

pigments or long-term fertilizers that crystallize poorly so that single-crystal X-ray diffraction is not applicable. X-ray diffraction on powders[13,14] is one approach to the analysis of these compounds[15] combined with calculations using previous knowledge. Another powerful technique for the analysis of such compounds is solid-state NMR spectroscopy.

In this study, polycrystalline DAB was initially studied by solid-state NMR spectroscopy because attempts to grow single crystals of DAB failed. This analytical approach was recently applied by us to methoxycarbonylurea (MCU), another promising long-term fertilizer.[16,17] In that case, single-crystal X-ray crystallography could not be applied because the single crystals of MCU obtained exhibit lattice disorder. Instead we resorted to standard[16] and more elaborate[17] techniques of solid-state NMR spectroscopy in combination with an isotope-labeling strategy and DFT calculations for structure elucidation ("NMR crystallography"). In this study on DAB, the results obtained by using these techniques were rather ambiguous compared with MCU owing to the inherent molecular symmetry of the primary structure of DAB. But routine solid-state NMR spectra of DAB revealed the existence of two polymorphic modifications of DAB. This shows one potential application of solid-state NMR spectroscopy for screening substances for (pseudo)polymorphism. Subsequent dynamic-solution NMR experiments on DAB in tetrahydrofuran revealed that the DAB molecule forms two configurations. With this knowledge, an optimized crystallization protocol was devised that finally has allowed the successful growth of DAB single crystals suitable for X-ray structure analysis. The X-ray structures show that the two polymorphic modifications of DAB are not formed as a result of the different configurations found in solution, but solely through crystal packing with different hydrogen-bonding patterns.

The rest of this article is organized as follows. First, a brief survey of the sample preparation and characterization is given, followed by our experimental set up, and a description of the experiments and calculations that were performed. Then the experimental results are presented, discussed, and summarized.

Experimental Section

Sample preparation: The synthesis of unlabeled and U-^{15}N-labeled DAB (U = ubiquitous) is described in detail in reference [18]. Selected configurations of DAB are shown in Figure 1. In summary, unlabeled DAB was synthesized by standard acetylation of biuret with a threefold excess of acetic anhydride catalyzed by 1 mL of a 65 % solution of SO_3 in sulfuric acid (yield 85–99 %). The precipitate was washed several times with water and then dried in vacuo. The resulting white powder melted at 203 °C.

For U-^{15}N-labeled DAB, the same synthesis was performed by using U-^{15}N-labeled biuret instead of unlabeled biuret (yield 91 %). U-^{15}N-Labeled biuret was synthesized by bubbling chlorine through a melt of U-^{15}N-labeled urea (purchased from Witega/Berlin, ^{15}N enrichment (99.2 ± 0.1) %). The product was recrystallized from water (yield 51 %). A small amount of byproduct was identified as U-^{15}N-labeled triuret by liquid-state ^{1}H NMR spectroscopy. Deuterated DAB ($^2H_3$-DAB) was produced by recrystallizing DAB from deuterium oxide and drying at 80 °C.

The polymorphic modification β-DAB was obtained by these synthetic procedures after recrystallization from water. The second polymorphic modification, α-DAB, was obtained by any of the following procedures: 1) tempering β-DAB at 150 °C for 1 day, 2) sublimation of β-DAB, and 3) recrystallization of β-DAB from tetrahydrofuran.

Solid-state NMR spectroscopy: Solid-state NMR spectra of powdered, polycrystalline samples were recorded with a home-built three-channel solid-state NMR spectrometer with an Oxford magnet at a field of 7 T and with a three-channel Varian InfinityPlus 14 T NMR spectrometer, as described in more detail in refs. [16,17]. The sample spinning frequency was stabilized to ± 1 Hz by using a spin-rate controller. $\pi/2$ pulse lengths of between 6.0 and 7.3 μs were chosen and pulse sequences were used with Hahn echo. In the experiments conducted at 7 T a standard CP-MAS sequence was used. All experiments performed with the 14 T machine employed TPPM decoupling[19] and ramped amplitude cross-polarization (RAMP-CP).[20]

^{13}C NMR chemical shifts are referenced[16] to tetramethylsilane (TMS) using external secondary shift standards: adamantane (δ = 29.50 and 38.56 ppm for the two adamantane signals[21]) or glycine (δ = 43.3 and 176.48 ppm for the two glycine signals[22]). ^{15}N NMR chemical shifts are referenced to solid NH_4Cl employing either an external sample of solid NH_4Cl or glycine using the expression $\delta(NH_4Cl,solid) - \delta(glycine,solid) = 6.4$ ppm.[23] For comparison with liquid-state ^{15}N NMR spectra with neat nitromethane as the external standard, the relation $\delta(CH_3NO_2,liq.) - \delta(NH_4Cl,solid) = 338.1$ ppm was employed.[24]

Liquid-state NMR spectroscopy: Liquid-state 1D NMR spectra were recorded with a Bruker AMX NMR spectrometer at room temperature operating at a magnetic field of 11.7 T. The chemical shifts are referenced to TMS (^{1}H, ^{13}C) or nitromethane (^{15}N). Calibration of the NMR spectra was performed by employing either a neat sample of nitromethane as ex-

ternal standard (^{15}N) or the following chemical shift values of solvent signals (^{1}H, ^{13}C). ^{1}H: 2.49 ppm (dimethyl sulfoxide, DMSO), 1.94 ppm (acetonitrile); ^{13}C: 39.51 ppm (DMSO), 1.39 ppm (acetonitrile).

Ab initio and DFT calculations: All quantum-chemical calculations of geometry, energy, vibrations, and ^{1}H, ^{13}C, and ^{15}N chemical shift tensors were carried out with the Gaussian 98 program.[25] The output was evaluated by using home-written programs in MATLAB[26] code.

Hartree–Fock (ab initio, data not shown) and B3LYP (density functional theory, DFT) methods were used combined with the 3-21G or 6-31G standard basis sets for initial geometry optimizations and then 6-31++G(d,p) in consideration of intramolecular hydrogen bonding. Vibrational frequencies were calculated to check that the geometries obtained correspond to (local) minima on the energy hypersurface. For chemical shielding calculations, the gauge-included atomic orbital (GIAO)[27,28] approach was used in conjunction with the 6-31++G(d,p) and 6-31++G(2d,2p) basis sets. The calculated chemical shielding values σ were converted to chemical shifts δ by using the ^{13}C absolute chemical shielding of TMS at 188.1 ppm[29] and the ^{15}N absolute chemical shielding of ammonia at 267.3 ppm calculated in the same way as described above.[16]

X-ray diffraction: Reflections were collected with a CCD Bruker-AXS Smart diffractometer with an ω scan at 173(2) (α-DAB) and 223(2) K (β-DAB) using graphite-monochromated $Mo_{K\alpha}$ radiation ($\lambda = 0.71073$ Å). The single crystals had the following dimensions: α-DAB: platelet, $0.7 \times 0.15 \times 0.05$ mm; β-DAB: needle, $0.50.06 \times 0.04$ mm. A total of 817 and 827 reflections were used in the θ range 4.2–30.5° and 3–30°, respectively. The crystal and refinement data were produced using the SHELXS-97[30] and SHELXL-97[31] programs (see Table 4). CCDC-620843 and CCDC-620844 contain the supplementary crystallographic data for this paper. These data can be obtained free of charge from The Cambridge Crystallographic Data Centre via www.ccdc.cam.ac.uk/data_request/cif.

Results and Discussion

Liquid-state NMR spectroscopy: DAB was dissolved in deuterated DMSO and acetonitrile. The chemical shifts obtained from the standard NMR spectra are presented in Table 1 and Table 2. The ^{13}C NMR chemical shifts are solvent-dependent with a downfield shift of around 1–2 ppm on going from DMSO to acetonitrile. Furthermore, a dynamic NMR study of DAB in deuterated tetrahydrofuran revealed the existence of two different configurations of DAB which show coalescence at low temperatures.[23] Preliminary and exemplary results are shown in Figure 2. The region of methyl-^{1}H signals reveals at 175 K two main signals that can be assigned to an asymmetric configuration of DAB and a single signal which shows that a symmetric configuration is also present. Similarly three plus two signals are observed in the region of NH chemical shifts for the asymmetric and symmetric configurations (not shown), respectively. The intramolecular dynamics between these two configurations were monitored by increasing the temperature, reaching the fast exchange limit at room temperature. The equilibrium constant was determined as $K = 5.6$ from the signal integrals of the spectrum at 175 K with the asymmetric configuration being more dominant.

Table 2. ^{15}N NMR isotropic chemical shifts [ppm, NH_3] of protonated and deuterated β-DAB (U-^{15}N,[D_3]DAB).[a]

Signal	Solid state			Liquid state	Calculation
	U-^{15}N DAB	[D_3]DAB	$\Delta\delta(^{15}N)$ [ppm]	in DMSO	DFT
a	105.1	104.1	−1.0	109.6	142.4
b	124.5	123.2	−1.3	130.8	163.2
c	127.6	126.8	−0.8		

[a] Accuracies are ±0.1 ppm. Liquid-state data obtained from U-^{15}N-DAB in DMSO.

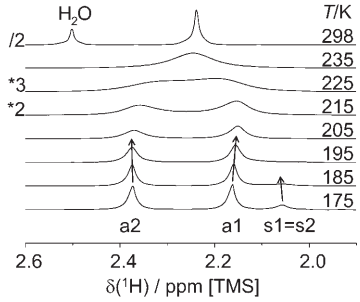

Figure 2. Liquid-state ^{1}H NMR spectra of DAB in THF at 11.7 T and at temperatures indicated on the right-hand side. Only the spectral region of methyl ^{1}H signals is shown. "s" indicates the signal of DAB in a symmetric configuration with six magnetically equivalent methyl-^{1}H nuclei. "a1" and "a2" indicate the signals of the two magnetically nonequivalent methyl groups in an asymmetric configuration.

Solid-state ^{13}C NMR spectroscopy

Results: Examples of ^{13}C (natural abundance) CPMAS NMR spectra are shown in Figure 3. Spectrum A is of U-^{15}N-labeled DAB (recrystallized from water) recorded at 14 T and with a MAS frequency of 6.667 kHz. The spectrum consists of six isotropic signals and their spinning sidebands. Isotropic signals were identified by variation of the spinning frequency and are labeled a–f. Spectra B–D in Figure 3 show the isotropic signals of the ^{13}C NMR spectra of different samples. Spectrum B corresponds to spectrum A with a slightly in-

Table 1. ^{13}C NMR chemical shifts of DAB in the solid and liquid states as well as values calculated by DFT.[a]

Signal no.	Type of carbon	Solid-state NMR δ(β-DAB) [ppm] (spectrum B)	Solid-state NMR δ(α-DAB)[ppm] (spectra C and D)	Liquid-state NMR δ [ppm] (in DMSO; in acetonitrile)	DFT (*ZEZZEZ* config.)
a	methyl	24.13	24.01	24.0; 25.0	19.7
b		25.55	24.56		
c	imide	148.3	152.6	149.2; 151.5	138.6
d		152.5			
e	amide	173.8	173.1	171.8; 173.3	159.4
f		177.3			

[a] In solution, each pair of carbon atoms a+b, c+d, and e+f is magnetically equivalent. The entries in each field of the last column show the solvent-dependency of the chemical shifts. Estimated accuracies are ±0.05 ppm for C(methyl) signals and ±0.1 ppm for other signals.

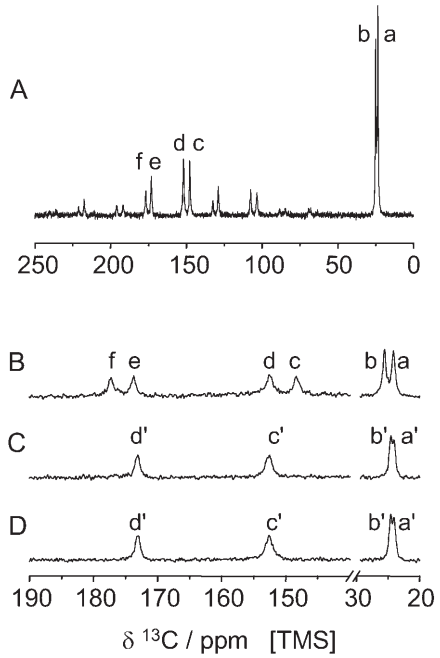

Figure 3. A) ^{13}C CPMAS NMR spectrum of U-^{15}N-labeled β-DAB at 14 T and a spinning speed of 6.667 kHz. Letters a–f indicate isotropic signals (see Table 1). B–D) ^{13}C CPMAS NMR spectra of unlabeled DAB at 14 T and a spinning speed of 8 kHz. Only the regions of isotropic signals are shown. B) β-DAB (recrystallized from water). C) α-DAB (produced from β-DAB tempered for 1 day at 150 °C). D) α-DAB (recrystallized from tetrahydrofuran). Letters a–f (a′–d′) indicate isotropic signals, as in spectrum A.

creased MAS frequency and is of unlabeled instead of U-^{15}N-labeled DAB.

Spectra C and D were obtained from DAB samples that have been prepared in different ways. The sample for spectrum C was prepared by tempering DAB for 1 day at 150 °C. The sample for spectrum D was obtained by recrystallization of DAB from tetrahydrofuran. Spectra C and D are practically identical. For subsequent discussion we introduce the names β-DAB (spectra A and B) and α-DAB (spectra C and D) to represent the two forms of DAB.

Spectrum B consists of six isotropic signals (a–f) and spectra C and D exhibit only four isotropic signals (a′–d′), although there are six carbon atoms in each DAB molecule. To assign the signals, the signal integrals have to be evaluated by summing the isotropic signals and corresponding spinning sidebands. With cross-polarization (CP) spectra, the evaluation of signal integrals is expected to give only a rough estimation because 1) the CP efficacy may be different for nonequivalent nuclei, for example, because of different numbers of neighboring hydrogen atoms, and 2) the CP efficacy is usually orientation-dependent, that is, it is different for the individual spinning sidebands. Nevertheless, in the present case the relative magnitudes of the signal integrals are very close to the integer values 1 and 2 with deviations of $<6\%$. In spectrum B, the relative sizes of the integrals are equal for all six signals. In spectra C and D, the ratio of the integrals is 1:1:2:2 for the signals a′, b′, c′, and d′. Thus, the two signals c and d of spectrum B correspond to the unresolved signal c′ in spectra C and D. Similarly the signals e and f correspond to signal d′ (see Table 1). Also the low-field C(methyl) signal in spectrum B is shifted to a position closer to the other C(methyl) signal. All the ^{13}C chemical shifts of α- and β-DAB are summarized in Table 1.

In addition, a slow-spinning ^{13}C (natural abundance) CPMAS NMR spectrum of U-^{15}N-labeled β-DAB at 14 T with a MAS frequency of 2 kHz was recorded (see Figure 4). Heteronuclear dipolar couplings between ^{13}C and

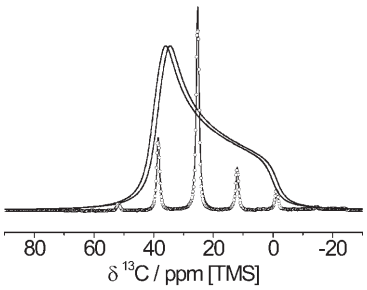

Figure 4. ^{13}C CPMAS NMR spectrum of U-^{15}N-labeled β-DAB at 14 T and a spinning speed of 2 kHz. Only the spectral region of the methyl-C signals is shown. The experimental sideband spectrum (dots) was processed with additional line-broadening which hides the symmetric splitting of each sideband. The fit of the sideband spectrum (solid line) yields $\delta_{aniso} = -25.1$ ppm and $\eta = -0.2$. By using these values and the experimental values $\delta_{iso} = 24.13$ and 25.55 ppm, the spectra of the static sample were calculated and are superimposed.

neighboring ^{15}N spins were of the order of 1.2 kHz. They are averaged to zero at the used MAS frequency, but information about the chemical shift anisotropy (CSA) is retained in the spinning sidebands. As each spinning sideband is a symmetrical doublet, the simulation was simplified by processing the spectrum with additional line-broadening. This leads to single Lorentzian lines for each spinning side band. The observation of six sidebands allows for an accurate simulation of the sideband spectra with the three CSA parameters $\delta_{iso} = (\delta_{xx} + \delta_{yy} + \delta_{zz})/3$, $\delta_{aniso} = \delta_{zz} - \delta_{iso}$, and $\eta = |\delta_{yy} - \delta_{xx}| / \delta_{aniso}$, where $|\delta_{zz} - \delta_{iso}| \geq |\delta_{xx} - \delta_{iso}| \geq |\delta_{yy} - \delta_{iso}|$.

The CSA tensors were simulated by using the SIMPSON program package.[32] For the simulation, the γ-COMPUTE method[33–36] was used in conjunction with the REPULSION set of 168 angles[37] and the simplex fitting method.[38] The best fit was obtained with $\delta_{iso} = 25.2$ ppm, $\delta_{aniso} = -25.1$ ppm, and $\eta = -0.20$ for the C(methyl) atom of β-DAB, with the uncertainties $\Delta\delta_{\alpha\alpha} = 2$ ppm ($\alpha = x,y,z$), $\Delta\delta_{aniso} = 2$ ppm, $\Delta\delta_{iso} < 1$ ppm, and $\Delta\eta = 0.1$. By employing the simulated CSA values for δ_{aniso} and η together with the experimental values $\delta_{iso} = 24.13$ and 25.55 ppm, spectra of the static sample were calculated and are superimposed as an envelope in Figure 4.

The extracted CSA tensor values are comparable to those of methyl carbon atoms in other molecules containing an acetyl group (see Table 3). The ratio of chemical shift aniso-

Table 3. Experimental CSA tensors for ^{13}C(methyl) atoms of DAB and related compounds containing acetyl groups from ref. [62,63], and also the results of DFT calculations on DAB in the *ZEZZEZ* configuration.

Methyl-^{13}C	δ_{iso} [ppm]	δ_{aniso} [ppm]	η
N,N″-diacetylbiuret (this study, SS-NMR, β-DAB)	25.2	−25.1	−0.20
N,N″-diacetylbiuret (this study, DFT)	19.7	−30.6	−0.65
acetaldehyde	33	−31	−0.39
acetone	30	−33	0.0
acetic acid	33	−23	0.0
acetic anhydride	25	−25	−0.12
methyl acetate	34	−12	−0.25

tropy and spinning speed (1.9) leads to a considerable deviation of the envelope of the spinning sidebands from the spectrum of the static sample (see Figure 4).

The spinning sideband patterns of the C(amide) and C(imide) signals are poorly resolved at the 2 kHz MAS frequency owing to unfavorable chemical shift differences and broad lines. Otherwise the number of sidebands at the 7 kHz MAS frequency is too low for an accurate simulation. These CSA tensors may be determined by a 2D experiment, as proposed in reference [39], but this technique is very time-consuming especially with the observation of ^{13}C in natural abundance and the rather long spin-lattice relaxation time of DAB.

Finally, ^{13}C (natural abundance)-^{15}N REDOR[40,41] spectra of U-^{15}N-labeled β-DAB were recorded (not shown). This technique allows direct measurement of internuclear distances through space up to around 5 Å in the case of ^{15}N,^{13}C pairs. The long-range distances can be used as constraints in the molecular modeling of the molecular conformation characterized by dihedral angles. In contrast to our previous experiments on MCU,[17] all long-range couplings in DAB are unfortunately overshadowed by the presence of strong one-bond couplings.

Discussion: The accuracy of the ^{13}C(methyl) chemical shifts is estimated to be 0.05 ppm and the signal-to-noise ratio to be 25 for the spectra in Figure 3. Therefore, impurities that may have formed in the course of the different sample preparations should be visible if they exceed 4%.

In view of the similar chemical shifts, the signals can be divided into three groups. The (mean) chemical shifts of the ^{13}C(methyl) and ^{13}C(imide) atoms are similar to those of the liquid-state NMR spectra (see Table 1). The largest chemical shift difference of 3.75 ppm is found for the ^{13}C(amide) atom between the mean of the two signals of β-DAB and the corresponding signal of DAB in DMSO.

The two different spectra for DAB result from different preparations of the sample. The nomenclature α- and β-DAB introduced above does not offer any explanation for the differences in the shifts or the number of ^{13}C signals. In principle, there are two possible explanations. 1) α- and β-DAB adopt different configurations. This probably also causes different crystal packing. 2) α- and β-DAB have the same configuration, but the crystal packing is different.

In addition, the possibility has to be considered that in β-DAB, two crystallographically nonequivalent, symmetric molecules fill the crystal unit cell, that is, the two molecules are magnetically nonequivalent. This possibility can be excluded by means of ^{15}N CPMAS NMR spectroscopy (see below). Furthermore, the chance of solvent molecules being part of the crystal structure has been excluded by ^{13}C NMR spectroscopy (excluding THF) and by elemental analysis (excluding water and THF).

In principle, ^{13}C CPMAS NMR spectra can be used to decide between the two explanations detailed above. The spectrum for β-DAB shows small

Table 4. Crystal data and structure refinement for α- and β-DAB.

	α-DAB	β-DAB
CCDC no.	620844	620843
empirical formula	$C_6H_9N_3O_4$	$C_6H_9N_3O_4$
formula weight	187.16	187.16
temperature [K]	173(2)	223(2)
wavelength [Å]	0.71073	0.71073
crystal system	monoclinic	monoclinic
space group	*P*21/*n*	*P*21/*c*
unit cell dimensions		
a [Å]	12.191(2)	4.4215(12)
b [Å]	5.3440(9)	20.224(6)
c [Å]	13.545(2)	9.300(3)
β [°]	112.401(3)	β = 93.496(6)
volume [Å^3]	815.9(2)	830.0(4)
Z	4	4
density (calcd) [Mg m^{-3}]	1.524	1.498
absorption coefficient [mm^{-1}]	0.129	0.127
F(000)	392	392
crystal size [mm^3]	0.7 × 0.15 × 0.05	0.50 × 0.06 × 0.04
ω range [°]	1.92–28.20	2.01–25.68
index ranges	$-13 \le h \le 16$	$-5 \le h \le 5$
	$-6 \le k \le 7$	$-24 \le k \le 24$
	$-17 \le l \le 17$	$-11 \le l \le 11$
reflections collected	4948	6743
independent reflections	1969 [R(int) = 0.0426]	1582 [R(int) = 0.0950]
completeness to θ = 28.20°	98.0%	100.0%
absorption correction	none	none
refinement method	full-matrix least-squares on F^2	full-matrix least-squares on F^2
data/restraints/parameters	1969/0/154	1582/0/155
goodness-of-fit on *F*2	1.028	1.049
final *R* indices [$I > 2\sigma(I)$]	R_1 = 0.0586 wR_2 = 0.1626	R_1 = 0.0448 wR_2 = 0.0963
R indices (all data)	R_1 = 0.0690 wR_2 = 0.1779	R_1 = 0.0754 wR_2 = 0.1085
largest diff. peak and hole [e Å^{-3}]	0.373 and −0.338	0.194 and −0.178

chemical shift differences between the pairs of chemically equivalent nuclei (1.4 ppm for C(methyl), 4.2 ppm for C(imide), and 3.5 ppm for C(amide)). These differences can be explained on the one hand by different configurations like, for example, in gluconamide with $\Delta\delta = 0.2$–2.9 ppm between the C(alcohol) and C(amide) nuclei[42] or $\Delta\delta =$ 10.3 ppm for the aromatic C1 atom in the two polymorphic modifications of dimethyl 3,6-dichloro-2,5-dihydroxyterephthalate.[43] On the other hand, different crystal packing can influence the number and strengths of the hydrogen bonds leading to chemical shift differences of the same magnitude, for example, values of $\Delta\delta$ of up to 4.6 ppm have been reported for the C(imide) nuclei in cyanuric acid and in a cyanuric acid/melamine co-crystal.[44] In this case, the main difference is that the neighboring O(imide) atoms are involved in one and two hydrogen bonds, respectively.

Explanation (1) is supported for DAB by the observation of a symmetric and an asymmetric configuration for DAB dissolved in THF (see above). Transferring this observation to the solid state, β-DAB would correspond to the most likely asymmetric configuration and α-DAB would correspond to the symmetric configuration. The observation of two signals for C(methyl) in the spectra of the symmetric α-DAB could be explained by slightly different surroundings of the two methyl groups. This means that each pair of C(amide), C(imide), and C(methyl) nuclei in the DAB molecule is crystallographically and hence magnetically nonequivalent. Similar splitting of the C(amide) and C(imide) signals is not observed because the chemical shift differences are very small and/or because of the larger linewidths of the C(amide) and C(imide) signals relative to the C(methyl) signals.

If explanation (2) is true, no conclusion can be drawn from the NMR data as to which kind of configuration (symmetric or asymmetric) might be present. On the one hand, the asymmetric configuration is favored for DAB in THF, but on the other hand, in the solid state, stronger intermolecular hydrogen bonds and a more compact crystal packing may favor the symmetric configuration.

Solid-state ^{15}N NMR spectroscopy: CSA tensors

Results: A ^{15}N CPMAS NMR spectrum of U-^{15}N-labeled β-DAB was recorded in order to gain information about the source of the six carbon lines observed for this compound. The spectrum is shown in Figure 5 (top of the left-hand panel). Three signals of roughly the same intensity can be observed. Two of them are relatively close to each other and the differences between the chemical shifts of these two signals and the third signal at a higher field are comparable to those observed in the liquid-state NMR spectrum (see Table 2). This slow-spinning spectrum was recorded at spinning frequencies of 1 kHz at 7 T (not shown) and 2 kHz at 14 T. With eight clearly resolved spinning sidebands in the spectrum at 14 T, the CSA tensors can be estimated by simulation. For this, the spectrum at 14 T was deconvoluted into three separate spectra (Figure 5a–c, left-hand panel). These

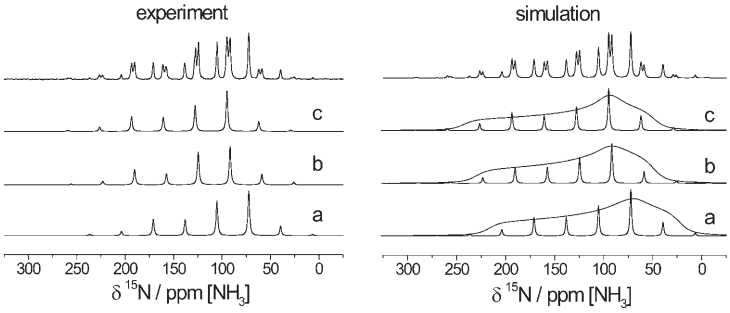

Figure 5. ^{15}N CPMAS NMR spectrum of U-^{15}N β-DAB at 14 T and spectral simulations. Left-hand side: Experimental spectrum and deconvoluted spinning sideband spectra of signals a, b, and c. Right-hand side: The corresponding simulations derived by using the SIMPSON program package (see text). The calculated spectra of a static sample are overlaid.

spectra were simulated using the SIMPSON program package[32] using the same conditions as described above for the simulation of the C(methyl) signals. The simulations are shown in the right-hand panel of Figure 5. Only minor deviations are found, especially for the spinning sidebands near the isotropic signal. These can be attributed to a lower CP efficacy for spins that are oriented near the magic angle with respect to the magnetic field B_0. In addition, the spectra of the static sample were calculated and are superposed on the simulated sideband spectra in Figure 5.

To compare the CSA tensors, it is most convenient to use the anisotropy parameter δ_{aniso} and the asymmetry parameter η. They are practically the same for all three signals: $\delta_{aniso} = 110(5)$ ppm for signals a and b, $\delta_{aniso} = 115(5)$ ppm for signal c, and $\eta = 0.40(5)$ for all three signals.

Next, ^{15}N (U-labeled) CPMAS NMR spectra were recorded for deuterated DAB at 14 T and 5 kHz spinning frequency (not shown). Deuterated DAB contains deuterated ND units and protonated methyl groups. Although the ^{1}H atoms directly bound to the ^{15}N atoms were replaced by ^{2}H atoms, cross polarization was possible through the ^{1}H-containing methyl groups. The signal at around 105 ppm is polarized less than the two low-field signals because the corresponding ^{15}N atom is more distant from the methyl groups than the other two ^{15}N atoms. Note that a secondary isotope effect on ^{15}N, $\Delta\delta(^{15}N) = \delta(ND) - \delta(NH)$, of the order of -1 ppm (see Table 2) is observable, which is probably caused by different zero-point energies in the anharmonic potential.

Discussion: The assignment of the ^{15}N signals of β-DAB was straightforward because the three signals are similar in intensity and there are three nitrogen atoms in the DAB molecule.

From the ^{13}C CPMAS NMR spectra the question arose as to whether two crystallographically nonequivalent, symmetric molecules fill the crystal unit cell of β-DAB. If this was the case, four ^{15}N signals with intensities of 1:1:2:2 would be expected. Therefore, the ^{15}N CPMAS NMR spectrum rules out this possibility.

The similarity of the three nitrogen atoms in β-DAB is reflected in the shape of the CSA tensors and the secondary

isotope effects on the ^{15}N atoms. The CSA tensors are comparable to those of acetanilide[45] and the fiber-modification of gluconamide[46] with respect to the isotropic ($\delta_{iso}=105$–127 ppm compared with 137 and 124 ppm, respectively) and the anisotropic chemical shifts ($\delta_{aniso}=110$–115 ppm compared with 108 and 115 ppm, respectively). Only the asymmetry parameters are considerably larger for DAB, with $\eta=0.4$ compared with 0.11 and 0.17, respectively. The CSA tensors for ^{15}N(imide) in methoxycarbonylurea[16] and phthalimide[47] show pronounced differences to these three tensors. There is no simple explanation for this behavior. Instead, there are a number of factors that influence the CSA tensors, like the degree of sp^2/sp^3 hybridization, conjugated double bonds (more delocalized bonding in the molecule), and the number and the strengths of the hydrogen bonds connected to the nitrogen atoms.

Variable-temperature ^{13}C and ^{15}N CPMAS NMR spectra

Results: As mentioned in the Experimental Section, at 150 °C an efficient conversion from β-DAB to α-DAB occurs. This raises the question: at what temperature does the conversion start? To partially answer this question we recorded the ^{13}C and ^{15}N CPMAS NMR spectra of β-DAB in the temperature range accessible by our MAS-NMR probe (152–353 K).

The upper panel in Figure 6 shows the ^{13}C CPMAS NMR spectra of β-DAB in the spectral region of the C(methyl) signals together with a simulation using two Lorentzian lines. Both signals are shifted by around 0.3 ppm in the direction of their mean upon increasing the temperature from 152 to 353 K, but they remain well separated without noticeable changes in their linewidth. This shows that at 353 K the interconversion from β-DAB to α-DAB is still not efficient.

The lower panel in Figure 6 shows the ^{13}C CPMAS NMR spectra of β-DAB in the spectral region of the C(amide) and C(imide) signals (spectra b in Figure 6). A small upfield shift is observed for the two C(amide) signals near 175 ppm. As the shift is small compared with the linewidth and as the signal-to-noise ratio is rather poor, the similar spectral regions of the most intense spinning sidebands are also shown in Figure 6 (lower panel, spectra a and c). Here, the same pattern is observed, yielding a consistent upfield shift of 0.3 ppm for both of the C(amide) signals on increasing the temperature from 152 to 353 K. In contrast, the chemical shifts of the C(imide) signals are temperature-independent in this temperature region.

In addition, ^{15}N CPMAS NMR spectra of U-^{15}N DAB (the α form) were recorded between 152 and 297 K with a MAS frequency of 2 kHz (spectra not shown). Low-field shifts of 0.1, 0.5, and 0.3 ppm for signals a, b, and c were observed in the spectra recorded between 152 and 297 K.

Discussion: As outlined in the previous sections, α-DAB is produced from β-DAB, for example, by tempering of the sample at 423 K. Therefore it is expected that the conversion of β-DAB into α-DAB takes place by molecular rearrangements in the crystal. In principle, such dynamics can be monitored by variable-temperature (VT) spectroscopy. In this case the available NMR equipment allowed only a moderate increase in temperature (152–353 K) compared with the temperature used for tempering. In the recorded VT NMR spectra, the two C(amide) and the two C(imide) signals show no coalescence, that is, the conversion into α-DAB cannot be monitored in this temperature range. Small shifts are observed in the spectra mainly for the atoms in the outer parts of the molecule, which can be explained by

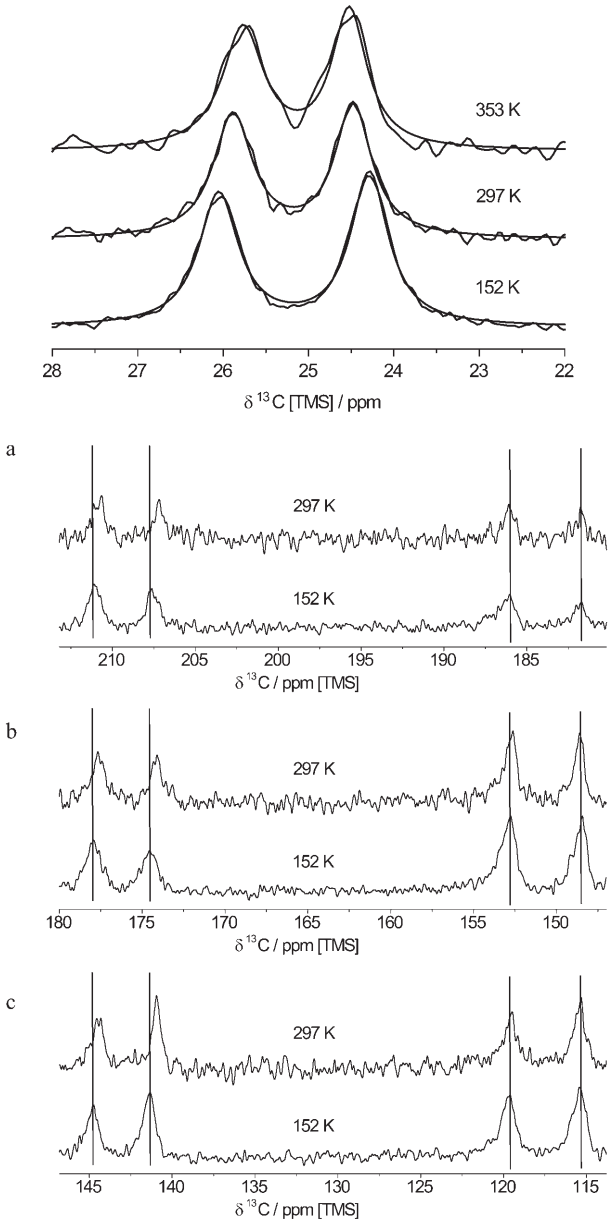

Figure 6. Top: ^{13}C CPMAS NMR spectra of β-DAB at 353, 297, and 152 K in the spectral region of the C(methyl) signals. Experimental spectrum and a simulation using two Lorentzian lines. Bottom: ^{13}C CPMAS NMR spectra of β-DAB at 297 and 152 K in the spectral region of the C-(amide) and C(imide) signals. a) Low-field spinning sidebands of the first order. b) isotropic signals. c) High-field spinning sidebands of first order.

the presence of stronger librations at higher temperatures which have an effect on the chemical shifts.

Ab initio and DFT calculations

Results: The results of ab initio and DFT calculations on DAB are similar and so only DFT results are reported herein. The calculated global minimum configuration of the isolated molecule is the asymmetric configuration (2*E*,3*Z*,4*E*,5*Z*,6*E*,7*Z*) (abbreviated below as *EZEZEZ*) (see Figure 1a). The calculations reveal a number of other possible configurations with higher electron energies. The next three configurations with increasing electron energies are shown in Figure 1b–d. These are the asymmetric configurations (2*Z*,3*E*,4*Z*,5*E*,6*Z*,7*Z*) and (2*E*,3*Z*,4*E*,5*Z*,6*Z*,7*E*), and the symmetric configuration (2*Z*,3*E*,4*Z*,5*Z*,6*E*,7*Z*) (abbreviated below as *ZEZZEZ*). The zero-point-corrected electron energies of these configurations relative to the most stable configuration are 4.04, 5.26, and 6.42 kcal mol^{-1}. The different configurations exhibit different patterns of N–H···O and C–H···O intramolecular hydrogen bonds and the carbon, nitrogen, and oxygen atoms in all four structures are planar. The symmetric configuration (Figure 1d) is characterized by a bifurcated intramolecular hydrogen bond at N′. Intermolecular hydrogen bonds were not included in the model. The configurations consistent with the experiments are *EZEZEZ* (Figure 1a) in THF solution and *ZEZZEZ* (Figure 1d) in the solid state (α- and β-DAB). Only the *ZEZZEZ* geometry was used in further calculations of the NMR parameters.

The calculated ^{13}C CSA data (referenced to TMS) are given in Table 1 and Table 2. The ^{15}N CSA data for the two types of ^{15}N nuclei together with the experimental values in brackets are given below (referenced to NH_3). Note, the average experimental values of δ_{iso} for N and N″ are given for convenience.

N′: $\delta_{iso,calcd} = 142.4$ ppm, $\delta_{aniso,calcd} = 100.1$ ppm, $\eta_{calcd} = 0.05$ ($\delta_{iso} = 105.1$ ppm, $\delta_{aniso} \approx 115$ ppm, $\eta \approx 0.40$).

N and N″: $\delta_{iso,calcd} = 163.2$ ppm, $\delta_{aniso,calcd} = 99.7$ ppm, $\eta_{calcd} = 0.51$ ($\delta_{iso} \approx 126.1$ ppm, $\delta_{aniso} \approx 110$ ppm, $\eta \approx 0.40$).

Discussion: The calculations reveal that the three most stable geometries of DAB in the gas phase are asymmetric and planar (apart from the methyl-H atoms). The symmetric configuration *ZEZZEZ*, which was observed by X-ray diffraction (vide infra), is favored in the crystal state as a result of a more efficient intermolecular hydrogen-bonding network. This also means that the calculations performed on single DAB molecules must be considered as approximate when compared with the experimental solid-state NMR data.

The ^{13}C CSA tensors are considered next. For the methyl groups, the differences between the calculated and experimental isotropic chemical shifts as well as the CSA tensors are 5–6 ppm. Thus a good agreement between calculation and experiment is obtained. Only an unusually high CSA tensor asymmetry is calculated which is not found in any comparable experimental CSA tensors (see Table 3). For C(imide) and C(amide), larger differences of 10–18 ppm between calculated and experimental isotropic chemical shifts are observed. These rather large differences in the chemical shifts can be explained by the absence of intermolecular hydrogen bonds in the model. Furthermore, NH distances may have been calculated as too long. Shorter calculated NH distances would lead to ^{15}N high-field shifts and ^{13}C low-field shifts for C(amide).

Next the ^{15}N CSA tensors are inspected. For the isotropic chemical shifts of the nitrogen atoms, large differences are observed between calculated and experimental values. These differences are in the opposite direction compared with those of the C(=O) spins. This observation therefore corroborates the explanation given above, namely the absence of intermolecular hydrogen bonds in the model. Furthermore, the differences between the calculated and experimental isotropic chemical shifts of the two types of nitrogen atoms are in very good agreement. Also the anisotropies of both types of nitrogen atoms and the asymmetry of N (and N″) agree well. Only the asymmetry of the N′ CSA tensor is not reproduced by the calculations. This may well be due to intermolecular hydrogen bonds which were neglected in the calculations.

X-ray diffraction

Results: The crystals of α- and β-DAB are both monoclinic (point group 2*m*) with space group *P*21/*n* for α-DAB and *P*21/*c* for β-DAB. In both cases, one DAB molecule ($C_6H_9N_3O_4$) forms the asymmetric unit. The cell volume of α-DAB is 1.7% smaller than that of β-DAB as a result of more compact packing (see Table 4). β-DAB has the symmetric configuration (2*Z*,3*E*,4*Z*,5*Z*,6*E*,7*Z*) (later abbreviated to *ZEZZEZ*) (Figure 7). The same molecular configuration is found for α-DAB (not shown). Slight deviations from planarity (apart from the H(methyl) atoms) and deviations from staggered conformations of the methyl groups are neglected here.

Concerning the spatial structure of the DAB backbone, as well as the term conformation as the term configuration could also be used. In principle, these two terms are characterized by a different rotational energy barrier between conformers (single bond) and configurational isomers (e.g., double bond).[48] As the backbone of DAB is made up of partial double bonds there is "hindered rotation". In addition, the rotational energy barrier is increased as a result of intra- and intermolecular hydrogen bonds. Therefore the term configuration seems to be more appropriate for DAB and will be used in the following.

The hydrogen-bond network of α- and β-DAB is depicted in Figure 8. Atom N1 refers to N, N2 to N′, and N3 to N″ (see Figure 7). The *ZEZZEZ* configuration of the DAB molecules in both modifications is fixed by the N2–H2···O2 and the N2–H2···O4 hydrogen bonds (H···O 1.91 Å) with N–H···O angles of around 133°. In both polymorphs the individual molecules are connected by a series of almost

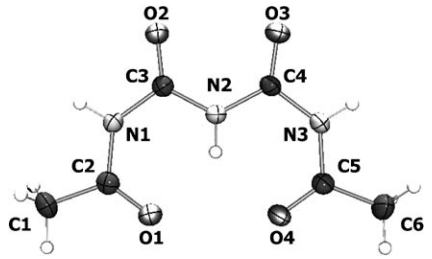

Figure 7. ORTEP representation[59] of a single molecule of β-DAB (asymmetric unit) with only non-hydrogen atoms labeled, as obtained from X-ray diffraction. The atoms are represented by 50% probability ellipsoids for thermal motion.

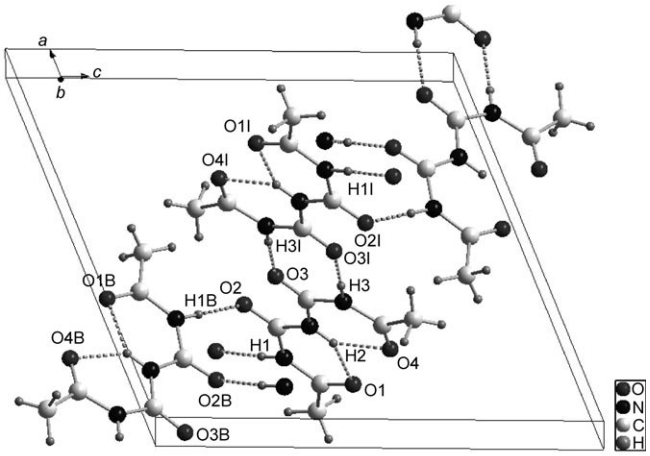

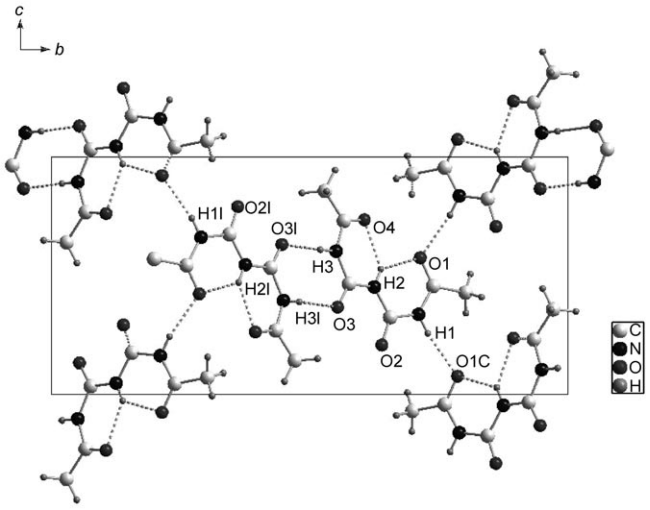

Figure 8. Top: Unit cell of α-DAB (DIAMOND[60,61]) viewed along 0–10. Symmetry operations used to generate the labeled hydrogen-bonded molecules I and B are $1-x,2-y,1-z$ and $0.5-x,0.5+y,0.5-z$. Bottom: Unit cell of β-DAB (DIAMOND) viewed along −100. Symmetry operations used to generate the labeled hydrogen-bonded molecules I and C are $3-x,1-y,1-z$ and $x,1.5-y,-0.5+z$.

linear N−H···O hydrogen bonds (e.g., 173° for N1−H1···O1 in α-DAB after normalization of NH and CH bond lengths to distances determined by neutron diffraction[49,50]). As a common feature two molecules related by inversion centers at 0,0,0 and 0.5,0.5,0.5 are connected by N3−H3···O3 hydrogen bonds (H3···O3 1.87 Å, N3−H3···O3 176° in α-DAB; 1.85 Å, 175° in β-DAB) forming a cyclic dimer. In α-DAB these dimers are hydrogen-bonded (H1···O 1.82 Å, N1-H1···O2 174°) to adjacent dimers generated by the two-fold screw axis forming hydrogen-bond helices along the crystallographic *b* axis. In β-DAB, however, the oxygen atom O2 is not involved in any hydrogen-bond network. In this case, the N1−H1···O1 hydrogen bond (H1···O1 1.87 Å, N1−H1···O 165°) interconnects the dimers to molecules generated by the *c*-glide plane. This results in less dense packing and thus a greater cell volume in β-DAB. The numbers of C−H··O contacts[51,52] (3.3–3.6 Å) for α- and β-DAB are given in Table 5. They are different for the two methyl groups in both polymorphic modifications.

Table 5. Numbers of N−H···O bonds (2.7–2.9 Å) and C−H···O contacts (3.3–3.6 Å) in α- and β-DAB.

	α-DAB		β-DAB	
	N−H···O	C−H···O	N−H···O	C−H···O
N1	1		1	
N2	2 (2 intra)		2 (2 intra)	
N3	1		1	
O1	1 (1 intra)	2	2 (1 intra)	1
O2	1	1		2
O3	1	1	1	1
O4	1 (1 intra)	1	1 (1 intra)	3
C1		3		4
C6		2		3

Discussion: The same configuration, namely the symmetric configuration *ZEZZEZ*, is found in both polymorphic modifications α- and β-DAB. This is in concordance with interpretation (2) of the ^{13}C CPMAS NMR spectra given above. The other interpretation (two different configurations as in THF solution) is ruled out by the X-ray diffraction results.

The degeneracy of each pair of atoms in the C_2-symmetric single molecule is lifted by the asymmetric environment in the crystal, that is, all atoms in the molecule are crystallographically unique. The main influence for this can be attributed to intermolecular hydrogen bonds. Inspection of Table 5 shows that these hydrogen bonds are distributed rather symmetrically in α-DAB with each oxygen atom forming one N−H···O bond. In contrast, in β-DAB, atom O1 forms two hydrogen bonds and O2 is not involved in any hydrogen bonding. Also the contacts between the oxygen atoms and the methyl groups are distributed more symmetrically in α-DAB than in β-DAB.

These results are in full agreement with the solid-state NMR data presented above. The ^{13}C CPMAS NMR spectrum of β-DAB shows six signals for six nuclei due to the asymmetric distribution of intermolecular hydrogen bonds. The same holds for the ^{15}N CPMAS NMR spectrum of β-DAB. For α-DAB, two signals are observed for the four C(=O) atoms which reflects the symmetric distribution of inter-

molecular hydrogen bonds. Note, however, that each pair of C(amide) and C(imide) nuclei are also crystallographically nonequivalent in α-DAB. They are only accidentally magnetically equivalent within the given spectral resolution. In contrast to the C(=O) atoms, the C(methyl) atoms in α-DAB give rise to two resolved signals which is in concordance with the X-ray diffraction structure because of the different number of contacts to oxygen atoms (see Table 5). With CO distances of 3.3–3.6 Å, these contacts also contribute to some extent to the stabilization of the structures, as in α-glycine and acetamide,[53] and they are in the range of typical CO distances of 3–4 Å.[54]

Conclusion

From the ^{13}C CPMAS NMR spectra of DAB prepared in different ways, it turned out that two polymorphic modifications can be obtained: β-DAB by recrystallization from water and α-DAB by 1) tempering of β-DAB at 150 °C, 2) sublimation, and 3) recrystallization from tetrahydrofuran. Interpretation of the ^{13}C and ^{15}N CPMAS NMR spectra together with elemental analyses lead to two possible explanations for the differences in α- and β-DAB: 1) The configuration and consequently probably the crystal packing is different or 2) the configuration is the same in both polymorphic modifications, but the crystal packing is different.

Furthermore, CSA tensors for the two C(methyl) atoms and for the three nitrogen atoms in β-DAB have been obtained from slow-spinning MAS spectra. Not only the CSA tensors of the two ^{13}C(methyl) atoms are similar, but also those of the three ^{15}N atoms. The ^{13}C(methyl) CSA tensor of β-DAB is in good agreement with those of similar molecules.

To further increase our understanding, especially of the ^{15}N CSA tensors, ab initio and DFT calculations were performed. The symmetric configuration *ZEZZEZ*, which was found later in α- and β-DAB by X-ray diffraction, was calculated as the fourth most stable geometry and features a bifurcated hydrogen bond. The three slightly more stable configurations are asymmetric and form different patterns of N−H···O and partly C−H···O bonds. The C(methyl) CSA tensor calculated for the symmetric configuration is in good agreement with the experimental CSA tensor, although a much larger asymmetry parameter was calculated. Good agreement is also observed for the anisotropy parameters of the CSA for all the nitrogen atoms and for the asymmetry of the CSA of N (and N″).

Variable-temperature (VT) ^{13}C and ^{15}N CPMAS NMR spectra of β-DAB were recorded in the temperature range 152–353 K. Small shifts were observed in the VT spectra mainly for the atoms in the outer parts of the molecule. A possible explanation for this observation is the presence of stronger librations at higher temperatures which have an effect on the chemical shifts. The conversion from β-DAB into α-DAB is too slow at the highest experimentally accessible temperature to show an effect in the dynamic NMR spectra.

By following an improved protocol, single crystals were obtained for both polymorphic modifications that were suitable for analysis by X-ray diffraction. The same symmetric configuration was observed in the crystals of both α- and β-DAB in contrast to DAB dissolved in THF in which an asymmetric and a symmetric configuration coexist. α- and β-DAB differ in their crystal packing. Analysis of the intermolecular N−H···O bonds and of the contacts between the oxygen atoms and the methyl groups allowed the chemical shifts in the ^{13}C CPMAS NMR spectra to be explained: In β-DAB the distribution of the intermolecular hydrogen bonds among the four oxygen atoms is asymmetric which leads to chemical shift differences of 3.5 ppm for C(amide) and 4.2 ppm for C(imide). In contrast, in α-DAB, each oxygen atom forms one N−H···O bond which leads to one NMR signal for both C(amide) spins and one signal for both C(imide) spins. The molecular packing is characterized in both polymorphic modifications by two kinds of intermolecular N−H···O bonds. One pattern gives a cyclic dimer in both α- and β-DAB, and often in amides as well.[55,56] The second pattern results in a two-fold screw axis in α-DAB and a *c*-glide plane in β-DAB. Ab initio calculations revealed three asymmetric configurations that are slightly more stable than the structure derived by X-ray diffraction. A more compact crystal packing and/or stronger intermolecular interactions seem to favor the symmetric configuration in the solid state.

Finally, interplay between solid-state NMR spectroscopy, quantum chemical calculations, and X-ray diffraction has allowed the detection of polymorphic modifications of a rather fundamental organic nature and their structural characterization. It is expected that a multitude of organic substances exist as a number of polymorphic modifications and this combined approach may be an interesting line to take in further investigations.

An issue for future studies on DAB is the determination of N−H bond lengths by solid-state NMR spectroscopy. For this, a correlation between the N−H bond length and the ^{15}N chemical shift, as obtained for collidine/acid dimers,[57] may be established and also used for related molecules like biuret and triuret. Finally, it would be interesting to study the kinetics of the phase transition from β-DAB to α-DAB and search for the presence of possible disordered intermediate structures. This could be accomplished by tempering experiments at an elevated temperature to speed up the transition in the crystallites followed by a rapid quenching of the temperature to freeze the structures as a function of the tempering time, similar to the study of slow-phase separation processes of adamantane in polystyrene.[58] From a kinetic analysis of these data it should be possible to estimate the activation barrier of the reaction.

Acknowledgements

Warm thanks to Hans-Heinrich Limbach, Mariusz Pietrzak, and Shasad Sharif for fruitful discussions. G.B. thanks the Deutsche Forschungsgemeinschaft for financial support. S.M. gratefully acknowledges a postdoctoral grant from DAAD (grant no. D/03/18809).

[1] C. B. Aakeröy, K. R. Seddon, *Chem. Soc. Rev.* **1993**, *22*, 397–407.
[2] G. R. Desiraju, *The Crystal As a Supramolecular Entity, Perspectives in Supramolecular Chemistry, Vol. 2*, Wiley, Chichester, **1996**, pp. 9–11.
[3] G. R. Desiraju, *Acc. Chem. Res.* **1996**, *29*, 441–449.
[4] B. Moulton, M. J. Zaworotko, *Chem. Rev.* **2001**, *101*, 1629–1658.
[5] M. U. Schmidt, *NATO ASI Ser., Ser. C* **1999**, *538*, 331–348.
[6] J. Haleblian, W. McCrone, *J. Pharm. Sci.* **1969**, *58*, 911–929.
[7] S. R. Vippagunta, H. G. Brittain, D. J. W. Grant, *Adv. Drug Delivery Rev.* **2001**, *48*, 3–26.
[8] J. Bernstein, *Polymorphism in Molecular Crystals, (International Union of Crystallography Monographs on Crystallography, Vol. 14*), Oxford University Press, Oxford, **2002**.
[9] W. Herbst, K. Hunger, *Industrial Organic Pigments*, VCH, Weinheim, **1993**.
[10] M. U. Schmidt, R. E. Dinnebier, *J. Appl. Crystallogr.* **1999**, *32*, 178–186.
[11] A. Burger, *Pharm Int.* **1982**, *3*, 158–163.
[12] K. R. Morris, *Drugs Pharm Sci.* **1999**, *95*, 125–181.
[13] K. D. M. Harris, M. Tremayne, *Chem. Mater.* **1996**, 8, 2554–2570.
[14] W. I. F. David, K. Shankland, N. Shankland, *Chem. Commun.* **1998**, 931–932.
[15] G. Lincke, *Dyes Pigm.* **2003**, *59*, 1–24.
[16] S. Macholl, F. Börner, G. Buntkowsky, *Z. Phys. Chem. (Muenchen Ger.)* **2003**, *217*, 1473–1505.
[17] S. Macholl, F. Börner, G. Buntkowsky, *Chem. Eur. J.* **2004**, *10*, 4808–4816.
[18] F. Börner, *Synthese, Charakterisierung und Untersuchung von schwerlöslichen Harnstoffderivaten als Grundlage für Düngemittel*, PhD Thesis, FU Berlin, Berlin, **2000**, p. 145.
[19] A. E. Bennett, C. M. Rienstra, M. Auger, K. V. Lakshmi, R. G. Griffin, *J. Chem. Phys.* **1995**, *103*, 6951–6958
[20] G. Metz, X. Wu, S. O. Smith, *J. Magn. Reson., Ser. A* **1994**, *110*, 219–227.
[21] W. E. Earl, D. L. VanderHart, *J. Magn. Reson.* **1982**, *48*, 35–54.
[22] S. Hayashi, *Magn. Reson. Chem.* **1999**, *37*, 843–851.
[23] S. Macholl, *Determination of Molecular Structures by Dipolar Solid State NMR Spectroscopy*, PhD Thesis, FU Berlin, Berlin, **2002**, p. 145.
[24] R. M. Claramunt, D. Sanz, C. Lopez, J. A. Jimenez, M. L. Jimeno, J. Elguero, A. Fruchier, *Magn. Reson. Chem.* **1997**, *35*, 35–75.
[25] Gaussian 98, M. J. Frisch, G. W. Trucks, H. B. Schlegel, G. E. Scuseria, M. A. Robb, J. R. Cheeseman, V. G. Zakrzeswski, J. A. Montgomery, R. E. Stratman, J. C. Burant, S. Dapprich, J. M. Millam, A. D. Daniels, K. N. Kudin, M. C. Strain, O. Farkas, J. Tomasi, V. Barone, M. Cossi, R. Cammi, B. Mennucci, C. Pomelli, C. Adamo, S. Clifford, J. Ochterski, G. A. Petersson, P. Y. Ayala, Q. Cui, K. Morokuma, D. K. Malick, A. D. Rabuck, K. Raghavachari, J. B. Foresman, J. Cioslowski, J. V. Ortiz, A. G. Baboul, B. B. Stefanov, G. Liu, A. Liashenko, P. Piskorz, I. Komaromi, R. Gomperts, R. L. Marin, D. J. Fox, T. Keith, M. A. Al-Laham, C. Y. Peng, A. Nanayakkara, C. Gonzalez, M. Challacombe, P. M. W. Gill, B. Johnson, W. Chen, M. W. Wong, J. L. Andres, C. Gonzales, M. Head-Gordon, E. S. Replogle, J. A. Pople, Gaussian, Inc., Pittsburg, PA, **1998**.
[26] MATLAB, The MathWorks, Inc., Natwick, MA, **1984–2000**.
[27] H. Fukui, *Prog. Nucl. Mag. Res.* **1997**, *31*, 317–342.
[28] K. Wolinski, J. F. Hinton, P. Pulay, *J. Am. Chem. Soc.* **1990**, *112*, 8251–8260.
[29] A. K. Jameson, C. J. Jameson, *Chem. Phys. Lett.* **1987**, *134*, 461–466.
[30] SHELXS-97, Program for Crystal Structure Solution, G. M. Sheldrick, Göttingen, **1997**.
[31] SHELXL-97, Program for Crystal Structure Refinement, G. M. Sheldrick, Göttingen, **1997**.
[32] M. Bak, J. T. Rasmussen, N. C. Nielsen, *J. Magn. Reson.* **2000**, *147*, 296–330.
[33] G. Eden, Y. K. Lee, M. H. Levitt, *J. Magn. Reson. Ser. A* **1996**, *120*, 56–71.
[34] M. Hohwy, H. Bildsoe, H. J. Jakobsen, N. C. Nielsen, *J. Magn. Reson.* **1999**, *136*, 6–14.
[35] M. H. Levitt, G. Eden, *Mol. Phys.* **1998**, *95*, 879–890.
[36] T. Charpentier, C. Fermon, J. Virlet, *J. Magn. Reson.* **1998**, *132*, 181–190.
[37] M. Bak, N. C. Nielsen, *J. Magn. Reson.* **1997**, *125*, 132–139.
[38] W. H. Press, B. P. Flannery, S. A. Teukolsky, W. T. Wetterling, *Numerical Recipes*, Cambridge University Press, Cambridge, **1986**.
[39] S.-F. Liu, J.-D. Mao, *J. Magn. Reson.* **2002**, *155*, 15–28.
[40] T. Gullion, J. Schaefer, *Adv. Magn. Reson.* **1989**, *14*, 57–83.
[41] T. Gullion, J. Schaefer, *J. Magn. Reson.* **1989**, *81*, 196–200.
[42] I. Sack, S. Macholl, J. H. Fuhrhop, G. Buntkowsky, *Phys. Chem. Chem. Phys.* **2000**, *2*, 1781–1788.
[43] M. Strohmeier, A. M. Orendt, D. W. Alderman, D. M. Grant, *J. Am. Chem. Soc.* **2001**, *123*, 1713–1722.
[44] K. Damodaran, G. J. Sanjayan, P. R. Rajamohanan, S. Ganapathy, K. N. Ganesh, *Org. Lett.* **2001**, *3*, 1921–1924.
[45] M. D. Lumsden, R. E. Wasylishen, K. Eichele, M. Schindler, G. H. Penner, W. P. Power, R. D. Curtis, *J. Am. Chem. Soc.* **1994**, *116*, 1403–1413.
[46] G. Buntkowsky, I. Sack, H.-H. Limbach, B. Kling, J. Fuhrhop, *J. Phys. Chem. B* **1997**, *101*, 11265–11272.
[47] W. L. Jarrett, C. G. Johnson, L. J. Mathias, *J. Magn. Reson. Ser. A* **1995**, *116*, 156–160.
[48] B. Testa, *Principles of Organic Stereochemistry*, Marcel Dekker, New York, **1979**.
[49] G. A. Jeffrey, L. Lewis, *Carbohydr. Res.* **1978**, *60*, 179–182.
[50] R. Taylor, O. Kennard, *Acta Crystallogr. Sect. B* **1983**, *39*, 133–138.
[51] T. Steiner, *Cryst. Rev.* **2003**, *9*, 177–228.
[52] T. Steiner, *Angew. Chem.* **2002**, *114*, 50–80; *Angew. Chem. Int. Ed.* **2002**, *41*, 48–76.
[53] Z. Berkovitch-Yellin, L. Leiserowitz, *Acta Crystallogr. Sect. B* **1984**, *40*, 159–165.
[54] G. R. Desiraju, *Acc. Chem. Res.* **1991**, *24*, 290–296.
[55] L. Leiserowitz, M. Tuval, *Acta Crystallogr. Sect. B* **1978**, *34*, 1230–1247.
[56] J. C. Williams, A. E. McDermott, *J. Phys. Chem. B* **1998**, *102*, 6248–6259.
[57] P. Lorente, I. G. Shenderovich, N. S. Golubev, G. S. Denisov, G. Buntkowsky, H.-H. Limbach, *Magn. Reson. Chem.* **2001**, *39*, S18–S29.
[58] G. Buntkowsky, M. Taupitz, E. Roessler, H. M. Vieth, *J. Phys. Chem. A* **1997**, *101*, 67–75.
[59] L. J. Farrugia, *J. Appl. Crystallogr.* **1997**, *30*, 565.
[60] G. Bergerhoff, M. Berndt, K. Brandenburg, *J. Res. Natl. Inst. Stand. Technol.* **1996**, *101*, 221–225.
[61] Diamond V3.1a, K. Brandenburg, Crystal Impact GbR, Bonn, **1997**.
[62] A. Pines, M. G. Gibby, J. S. Waugh, *Chem. Phys. Lett.* **1972**, *15*, 373–376.
[63] J. S. Waugh, M. G. Gibby, A. Pines, S. Kaplan, *Proceedings of the 17th Colloque Ampere*, North-Holland Publishing Company, Amsterdam, **1972**, p. 13.

Received: December 21, 2006
Revised: February 18, 2007
Published online: May 7, 2007

